Anal. Chem. **XXXX,** *xxx,* 000–000

Three-Dimensional Time-of-Flight Secondary Ion Mass Spectrometry Imaging of a Pharmaceutical in a Coronary Stent Coating as a Function of Elution Time

Gregory L. Fisher,*,† Anna M. Belu,‡ Christine M. Mahoney,§ Klaus Wormuth,|| and Noriaki Sanada⊥

Physical Electronics, Incorporated, 18725 Lake Drive East, Chanhassen, Minnesota 55317, Medtronic, Incorporated, 710 Medtronic Parkway LT130, Minneapolis, Minnesota 55432, National Institute of Standards and Technology, 100 Bureau Drive MS8371, Gaithersburg, Maryland 20899, SurModics, Incorporated, 9924 West 74th Street, Eden Prairie, Minnesota 55344, and ULVAC-PHI, Incorporated, 370 Enzo, Chigasaki City, Kanagawa 253-8522, Japan

Three-dimensional (3D) chemical images reveal the surface and subsurface distribution of pharmaceutical molecules in a coronary stent coating and are used to visualize the drug distribution as a function of elution time. The coronary stent coating consists of 25% (w/w) sirolimus in a poly(lactic-*co*-glycolic acid) (PLGA) matrix and is spray-coated onto metal coupons. Information regarding the 3D distribution of sirolimus in PLGA as a function of elution time was obtained by time-of-flight secondary ion mass spectrometry (TOF-SIMS) imaging using a Au^+ ion beam for analysis in conjunction with a C_{60}^+ ion beam for sputter depth profiling. The examined formulation is shown to have large areas of the surface as well as subsurface channels that are composed primarily of the drug, followed by a drug-depleted region, and finally, a relatively homogeneous dispersion of the drug in the polymer matrix. Elution is shown to occur from the drug-enriched surface region on a relatively short time scale and more gradually from the subsurface regions of homogeneously dispersed drug. Bulk composition was also probed by X-ray photoelectron spectroscopy (XPS) depth profiling and confocal Raman imaging, the results of which substantiate the TOF-SIMS 3D images. Finally, the effectiveness of a C_{60}^+ ion beam for use in 3D characterization of organic systems is demonstrated against another polyatomic ion source (e.g., SF_5^+).

Coronary implants that feature a drug delivery system have been developed to address the problem of restenosis (reblockage) following placement of an arterial stent.[1] In such drug delivery devices, a polymer is commonly used as the excipient for the pharmaceutical agent. The release rate of the pharmaceutical may be controlled by the formulation of the drug/polymer coating and the dispersion of the drug in the polymer matrix.[2] Moreover, since the drug delivery device will be in contact with human tissue, it is important to understand the surface chemistry because it strongly influences the biocompatibility of the device. Ideally, the device should be inert to the immune system, otherwise thrombosis may occur. For these reasons, it is important to characterize in vivo drug delivery devices and to relate the chemical and physical properties to how the implant will function over time. The present study focuses on the three-dimensional (3D) characterization of a drug-eluting stent coating that is composed of 25% (w/w) sirolimus in a poly(lactic-*co*-glycolic acid) (PLGA) matrix. The goal is not to assess the biocompatibility of a device or of the drug/polymer coating but, rather, to visualize the lateral and depth distribution of the drug in the polymer matrix and to relate the drug distribution to the elution rate. To this end, we have employed time-of-flight secondary ion mass spectrometry (TOF-SIMS) imaging, and we report here the first full 3D visualization of the chemical constituents in a pharmaceutical bearing coronary stent coating as a function of elution time. We will also briefly compare and contrast the qualities offered by distinct sputter ion beams for probing molecular distributions beyond the sample surface.

In the past decade, Raman imaging has been employed to understand the structure of polymer composites in the field of biomaterials.[3,4] The incorporation of high-sensitivity detectors has permitted Raman imaging analyses to be carried out in a useful time period (i.e., minutes instead of hours). More recently, confocal Raman imaging has been used to probe certain materials in three dimensions (e.g., films) in addition to surface characterization. The primary limitations of Raman imaging, including confocal, are spectral interferences arising from similar material chemistries, weak signal intensities, and a depth resolution on the order of 250 nm. TOF-SIMS provides the capability to differentiate similar chemistries based on mass spectrometry in conjunction with high-resolution imaging. Moreover, the lateral distribution of component chemistries may be probed as a function of depth with a resolution of several nanometers. The first reported

* To whom correspondence should be addressed. E-mail: gfisher@phi.com.
† Physical Electronics, Incorporated.
‡ Medtronic, Incorporated.
§ National Institute of Standards and Technology.
|| SurModics, Incorporated.
⊥ ULVAC-PHI, Incorporated.

(1) Ge, L.; Iakovou, I.; Cosgrave, J.; Chieffo, A.; Montorfano, M.; Michev, I.; Airoldi, F.; Carlino, M.; Melzi, G.; Sangiorgi, G. M.; Corvaja, N.; Colombo, A. *Eur. Heart J.* **2005**, *26*, 1056–1062.
(2) Belu, A.; Mahoney, C.; Wormuth, K. *J. Controlled Release* **2008**, *126*, 111–121.
(3) Clarke, F. C.; Jamieson, M. J.; Clark, D. A.; Hammond, S. V.; Jee, R. D.; Moffat, A. C. *Anal. Chem.* **2001**, *73*, 2213–2220.
(4) Kang, E.; Wang, H.; Kwon, I. K.; Robinson, J.; Park, K.; Cheng, J.-X. *Anal. Chem.* **2006**, *78*, 8036–8043.

10.1021/ac901587k CCC: $40.75 © XXXX American Chemical Society

use of TOF-SIMS with a C_{60}^+ ion beam to characterize a drug-loaded polymer was reported by Braun and co-workers.[5,6] The drug/polymer system under interrogation consisted of 8.8% (w/w) paclitaxel in poly(styrene-*b*-isobutylene-*b*-styrene) (SIBS). Sputter rates were measured to be in the range of 1.9 and 19 nm/s, depending on the primary ion beam current. This study demonstrated that, using a C_{60}^+ ion beam for sputter erosion of organic material, a drug-loaded polymer matrix may be characterized well into the micrometer scale (~2 μm) while still maintaining the molecular and fragment ion signals characteristic of both the drug and the excipient. This study also demonstrated that, following C_{60}^+ ion beam sputtering to micrometer-scale depths, the phase distribution of the molecular components was not significantly altered and there was little topographic evolution as a function of sputtered depth. These results clearly indicate that a drug/polymer system may be probed at depth by C_{60}^+ ion sputtering without altering the intrinsic distribution of either the drug or the polymer.

An initial TOF-SIMS characterization of sirolimus in PLGA has been reported by Mahoney et al.[7] wherein spin-cast thin films of sirolimus and PLGA were interrogated along with 5%, 25%, and 50% (w/w) formulations of sirolimus in PLGA. This seminal work has established the metrics for differentiation of the drug and the polymer in sirolimus/PLGA formulations and represents the first demonstration of depth profiling this drug/polymer system with a cluster ion beam. The negative secondary ion polarity (−SIMS) reference spectra were not provided in this article and so are provided here as Supporting Information.[8] Briefly, the distinguishing mass spectral features of sirolimus are $C_5H_{10}N^+$ (84 *m/z*, +SIMS) and CN^- (26 *m/z*, −SIMS), and those of PLGA are $C_3H_4O^+$ (56 *m/z*, +SIMS) and $C_3H_5O_2^-$ (73 *m/z*, −SIMS). As may be observed in the reference spectra, there are a number of mass spectral features that are characteristic of either sirolimus or PLGA.

Mahoney et al. utilized an SF_5^+ polyatomic ion beam for depth profiling of the sirolimus/PLGA films in order to collect 2D images-at-depth and reveal the subsurface distributions of both sirolimus and PLGA in the as-cast coating. The sample temperature was maintained at −100 °C during depth profile analysis to minimize the sputter ion-induced artifacts and to achieve nominal uniformity in the sputter rate. Valuable insights from this work include the observation that the sputter rates of sirolimus and PLGA using an SF_5^+ ion beam are nearly equivalent under temperature-controlled conditions and the less obvious realization that sirolimus is more susceptible to SF_5^+ ion-induced damage than is PLGA. Characterization of the stent coating as a function of elution was not reported.

Concurrently, Belu et al.[2] utilized a multitechnique approach by combining TOF-SIMS, X-ray photoelectron spectroscopy (XPS), and confocal Raman microscopy to characterize the 5%, 25%, and 50% (w/w) formulations of sirolimus in PLGA and to elucidate the effects of drug elution on the morphology of the spin-cast coatings. In their study, it was observed that the formulation had a profound effect on the characteristics of drug elution; specifically, it was revealed that formulations of greater sirolimus content resulted in a large initial release of the drug on a relatively short time scale. Confocal Raman microscopy was used to probe the morphology of the 25% (w/w) sirolimus in PLGA coating as a function of elution time. These images reveal that the coating thickness is reduced on a short time scale as the drug elutes and via hydrolytic decomposition of the polymer matrix at elution times >30 days, in a manner that is consistent with prediction. The TOF-SIMS measurements were limited to the near-surface region (≤500 nm) of the sirolimus/PLGA formulations prior to elution, and XPS analysis was restricted to quantitation at the surface of the sirolimus/PLGA formulations prior to elution.

The capability to visualize 3D chemical information as a function of elution time, in conjunction with the elution profiles, is an effective tool that may be used to enhance the design of in vivo drug delivery systems. The elution curve of the 25% (w/w) formulation of sirolimus in PLGA examined in the present study reveals that much of the drug (~55%) has eluted in the first day. Therefore, the 3D chemical distributions of a control (time zero) sample and two samples that were eluted for 1 h and 1 day, respectively, are examined. 3D characterization was accomplished by TOF-SIMS imaging using a Au^+ ion beam for analysis in conjunction with a C_{60}^+ ion beam for sputter depth profiling. The salient features of the TOF-SIMS 3D images of the control (time zero) sample are supported by XPS depth profile and confocal Raman image data acquired on alternate control samples.

The analytical advantage of TOF-SIMS lies in the ability to obtain submicrometer (ca. <200 nm) spatially resolved molecular information from the surface region of the probed specimen. Constituents of the interrogated sample are differentiated by the respective mass-to-charge (*m/z*) ratios of features in the mass spectra. By way of comparison, analysis by XPS or confocal Raman provides chemical state information, or functional group chemistries, at spatial resolutions of >5 μm and ~250 nm, respectively. An inherent difficulty is encountered, which may obfuscate interpretation of the data, when a chemical functionality is present in more than one component of the interrogated specimen. Nevertheless, these spectra are typically straightforward to interpret. Finally, the detection sensitivity and lateral resolution of XPS and confocal Raman microscopy are inferior to those attainable by TOF-SIMS.

Recent applications involving TOF-SIMS analysis of biological specimens and biomaterials have shown that much of the valuable chemical information lies below the probed surface. Such examples highlight the necessity for 3D molecular imaging by TOF-SIMS. However, the static limit, broadly defined as the primary ion dose beyond which artifacts are introduced via ion beam-induced damage to analyte molecules,[9−12] had formerly limited the ability to probe molecular information at depth. Notwithstanding, the recent advent of a high-voltage C_{60}^+ molecular ion source is an enabling technology for the beyond-the-static-limit ap-

(5) Braun, R. M.; Cheng, J.; Parsonage, E. E.; Moeller, J.; Winograd, N. *Appl. Surf. Sci.* **2006**, *252*, 6615–6618.
(6) Braun, R. M.; Cheng, J.; Parsonage, E. E.; Moeller, J.; Winograd, N. *Anal. Chem.* **2006**, *78*, 8347–8353.
(7) Mahoney, C.; Fahey, A.; Belu, A. *Anal. Chem.* **2008**, *80*, 624–632.
(8) Supporting Information to this manuscript available via the Internet.
(9) Winograd, N. *Anal. Chem.* **2005**, *77*, 143A–149A.
(10) Winograd, N.; Postawa, Z.; Cheng, J.; Szakal, C.; Kozole, J.; Garrison, B. *Appl. Surf. Sci.* **2006**, *252*, 6836–6843.
(11) Cheng, J.; Wucher, A.; Winograd, N. *J. Phys. Chem. B* **2006**, *110*, 8329–8336.
(12) Fletcher, J. S.; Conlan, X. A.; Jones, E. A.; Biddulph, G.; Lockyer, N. P.; Vickerman, J. C. *Anal. Chem.* **2006**, *78*, 1827–1831.

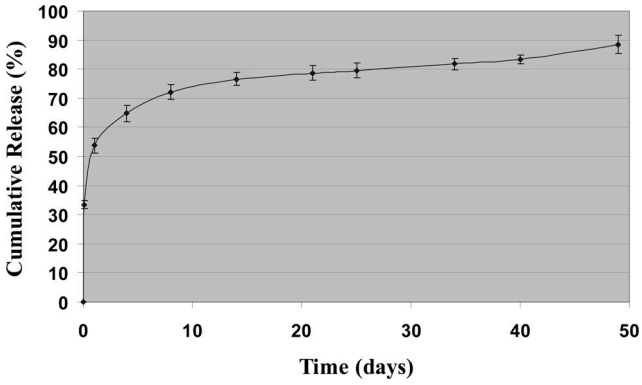

Figure 1. Elution curve of 25% (w/w) sirolimus in PLGA spray-applied thin films showing the cumulative release of sirolimus over 50 days. The error bars represent one standard deviation based on five measurements at each time interval.

plications of TOF-SIMS that allows the investigator to interrogate the chemical composition and molecular distribution of a specimen well beyond the surface region. The <10 nm depth resolution that is attainable by depth profiling with a molecular C_{60}^+ sputter ion beam is superior to the ~250 nm pixel size afforded by confocal Raman microscopy.

EXPERIMENTAL SECTION

See the disclaimer clause in the Acknowledgments.

Samples. Multiple samples consisting of 25% (w/w) sirolimus in a PLGA matrix were prepared for elution and subsequent analysis. The sirolimus, also commonly identified as rapamycin, was obtained from ZYF Pharm Chemical (Shanghai, China). The PLGA (50:50 lactide/glycolide), with a molecular weight (M_n) given as a range of 40−75K, was obtained from Sigma (St. Louis, MO). Both chemicals were used without further treatment or purification. The elution coatings were made by spray coating the sirolimus/PLGA formulation onto MP35N alloy coupons and allowing the coatings to dry in air. The quantity of the applied sirolimus/PLGA formulation was equivalent to that required to form a ~7 μm thick film in order to simulate the coating on a coronary stent.

Drug Elution. Several control (time zero) samples were held aside for analysis. The balance of the samples were eluted to various time intervals, and several samples were produced at each elution interval for subsequent analysis. The elution medium consisted of Tris-buffered saline solution (pH 8.0) that was diluted to 10 mM followed by addition of 0.4 wt % sodium dodecyl sulfate and, finally, buffered to pH 7.4 with 1 N HCl. The Tris-buffered saline and the sodium dodecyl sulfate were acquired from Sigma (St. Louis, MO). The samples were incubated at 37 °C with gentle agitation. The elution volume was 3 mL, and the entire volume was sampled and replenished at each time interval. The elution curve was generated by measuring the quantity of drug released into the buffered solution from the coupon at time intervals of 1 h and 1, 4, 8, 14, 21, 25, 34, 40, and 49 days. The quantity of drug released into the buffered solution was determined by measuring the UV absorption at 278 nm using an HP diode array spectrophotometer. The elution data (Figure 1) indicates that the most pronounced change occurs in the first day of elution. Therefore, the samples that are discussed in this article are limited to the control (time zero), the one-hour elution, and the one-day elution specimens.

TOF-SIMS Analysis. TOF-SIMS analysis was performed using a Physical Electronics (Chanhassen, MN) TRIFT V nanoTOF that is equipped with a 30 kV liquid metal ion gun (LMIG) and a 20 kV C_{60} primary ion gun. The LMIG and the C_{60} gun were employed in a dual-beam configuration to collect the depth profile and the 3D image data; the LMIG was operated in the pulsed mode to probe the lateral distribution of chemical moieties, and the C_{60} gun was operated in the dc mode to remove multiple layers of material from the sample surface between analytical cycles. The LMIG column is oriented at 40° from surface normal and is operated such that the sample is interrogated by a mass-pure Au^+ analytical ion beam. The pulsed current of the Au^+ primary ion beam was 0.037 pA, and the analytical field of view (FOV) was 200 μm × 200 μm. A primary ion dose density (PIDD) of 1.8×10^{11} Au^+/cm^2, averaged over 256 × 256 image pixels, was delivered to the sample during each analysis cycle. The C_{60} column is oriented 48° from surface normal. A 1 nA dc current of mass-pure C_{60}^+ was delivered into a 400 μm × 400 μm raster area resulting in a PIDD of 2.3×10^{15} C_{60}^+/cm^2 during each sputter cycle. The sputter rate of the sirolimus/PLGA formulation is an approximation (~15.1 nm^3/C_{60}^+) based on the results obtained using both bulk polymer and thin-film polymer samples of known thickness under similar analytical conditions; the sputter rates of sirolimus and PLGA have been shown previously to be similar.[7] Data in the positive and the negative secondary ion polarities were collected from different areas of the samples that were utilized in this study. The total time for each depth profile/3D image acquisition of the control (time zero) sample was approximately 9 h, and for each of the eluted specimens it was approximately 4 h. In the course of each acquisition, mass spectral information at each image pixel was collected in the m/z range of 0−1850 m/z and saved in a raw data stream file. Saving the complete mass spectrum of each image pixel over the course of the depth profile allows off-line data reduction (i.e., retrospective analysis) and generation of 3D images. Charge compensation was achieved using 10 eV electrons during both the analysis and the sputter phases of the depth profile acquisition. All samples were nominally held at room temperature throughout the depth profile analysis. Note: generation of 3D isosurface images was accomplished using a proprietary software package, WinCadenceN, from Physical Electronics (Chanhassen, MN).

A comparison of the potential for 3D chemical imaging applications related to the use of either C_{60}^+ or SF_5^+ as the dc sputter source is discussed in this article; this evaluation is based on image data of the control (time zero) sample only. The data presented in this article wherein SF_5^+ was used as the dc sputter source was collected on a different instrumental platform than is described above, and the reader is directed to a recent publication for a full description of the hardware and the analytical conditions.[7] Briefly, mass-pure 25 kV Bi_3^+ (0.3 pA pulsed current) and 5 kV SF_5^+ (6 nA dc current) ion beams were used for depth profile and image acquisition. The raster areas of the dc sputter and the pulsed analysis beams were 500 μm × 500 μm and 200 μm × 200 μm, respectively. A PIDD

of 2.3×10^{10} Bi_3^+/cm^2, averaged over 128×128 image pixels, was delivered to the sample during each analysis cycle, and a PIDD of 2.3×10^{14} SF_5^+/cm^2 was delivered to the sample during each sputter cycle. Charge compensation was achieved using low-energy electrons (~25 eV) during both the analysis and the sputter phases of the depth profile acquisition, and the sample was nominally held at −100 °C during analysis.

Confocal Raman Microscopy. A WITec (Ulm, Germany) CRM 200 scanning confocal Raman microscope, equipped with a Nd:YAG laser at 532 nm and a piezoelectric stage, was utilized in the Raman imaging mode. The laser light was focused into the sample using a 100× dry objective (numerical aperture 0.90). The laser spot was scanned over the sample so that, at 0.250 μm intervals, a Raman spectrum was collected over the spectral region of 500−3500 cm^{-1} with an integration time of 0.3 s per spectrum. Confocal optics allowed cross-sectional imaging of the coating (perpendicular to the coating surface) over a region of 60 μm wide by 5 μm deep, generating an image of 240×20 pixels with a full spectrum at each pixel. These 4800 spectra were analyzed with an augmented classical least-squares algorithm using the reference spectra of pure sirolimus, both amorphous and crystalline, and pure PLGA. This analysis converted the spectra into relative signal intensities of the pure sirolimus and pure PLGA components at each pixel resulting in images that show the spatial distribution of the drug and the excipient. For the sample examined here, only amorphous sirolimus was detected. The reader is directed to a recent publication for a more thorough description of the confocal Raman method.[2]

XPS Analysis. X-ray photoelectron spectroscopy depth profile analysis was accomplished using a Physical Electronics (Chanhassen, MN) Quantera SXM scanning X-ray microprobe equipped with a 10 kV C_{60}^+ sputter ion gun oriented 76° from surface normal. The X-ray probe used for these measurements was composed of monochromatic Al Kα photons (15 kV, 25 W) having a beam diameter of 100 μm. Survey spectra were obtained operating the energy analyzer at a 280 eV pass energy and a 53° takeoff angle. High energy resolution C 1s, N 1s, O 1s, and Si 2p spectra were obtained during the depth profile analysis using pass energies of 26, 224, 112, and 224 eV, respectively, at a 70° takeoff angle. A step size of 0.1 eV was utilized for the C 1s and N 1s regions, and a step size of 0.2 eV was utilized for the O 1s and Si 2p regions. Over the C, N, O, and Si energy windows, the number of sweeps during each analysis cycle were 6, 3, 2, and 2, respectively. During the depth profile, a C_{60}^+ sputter ion beam with a dc current of approximately 10 nA was rastered over an area of 2 mm × 3 mm. A total sputter time of 80 min was used to collect the depth profile data: 10 cycles at 1 min duration, 10 cycles at 2 min duration, and 10 cycles at 5 min duration. The total sputtered depth is estimated at approximately 800 nm based on the sputter rate of a similar polymer (e.g., PMMA). Charge neutralization was accomplished during analysis using a combination of 1 eV electrons and 7 eV Ar^+ ions; no charge compensation was employed during the sputter phase of the depth profile.

RESULTS AND DISCUSSION

The elution curve of the spray-applied 25% (w/w) sirolimus in PLGA coating is given in Figure 1. Release of the drug was monitored over the course of 49 days. There is an obvious initial surge of drug from the coating into the elution medium that occurs within the first day. This elution behavior is markedly different from that observed for the spin-cast coating of the same formulation.[2] The drug release from the spray-applied coatings utilized in this study accounts for almost 55% of the drug in the coating; it seems reasonable that this initial release of drug would account for a significant portion of the morphological change that occurs in the film. Thus, for the purposes of this study, we focus on characterizing the changes related to the surface and subsurface distributions of sirolimus and PLGA in the first day of elution using a control (time zero) sample and samples that were eluted for 1 h and 1 day. We have imaged and depth-profiled these samples by TOF-SIMS using a Au^+ ion beam for analysis and a C_{60}^+ ion beam for sputtering. In this way we are able to visualize both the lateral distributions, via the 2D images-at-depth, and the 3D distributions of both sirolimus and PLGA within the sputter depth-profiled region of the coatings.

The TOF-SIMS depth profiles of the control, one-hour, and one-day elution samples are shown in Figure 2. The $C_5H_{10}N^+$ and CN^- secondary ions which are diagnostic of sirolimus, the $C_3H_4O^+$ and $C_3H_5O_2^-$ secondary ions which are diagnostic of PLGA, and the Na^+ secondary ions are monitored as a function of sputtered depth in each sample. There are higher mass ions that are characteristic of the profiled components of drug and polymer, particularly in the case of sirolimus. However, the characteristic ions of sirolimus and PLGA shown in the depth profiles and utilized for 3D imaging were those having the best signal-to-background with which to achieve high-contrast imaging.[8] The depth scale is approximated based on the sputter rates of bulk and spin-cast polymers (~15.1 nm^3/C_{60}^+) and is similar to the sputter rates shown previously for sirolimus and PLGA.[7] For the purpose of making a succinct, qualitative comparison of the effects of elution, only the CN^-, $C_3H_5O_2^-$, and Na^+ secondary ion signals as a function of sputtered depth are shown for the one-hour and one-day elution samples. For each secondary ion that is monitored, each data point of the depth profile is a sum of the counts of that species across the entire raster frame, i.e., 200 μm × 200 μm. So, the depth profile represents the average quantity of each component as a function of depth. It should be noted that depth profiles in each secondary ion polarity were carried out on different portions of the same sample. The coatings are rather heterogeneous, and so the profiles of sirolimus and PLGA have different average concentration gradients below the surface at any given point of a particular sample. Nevertheless, there are qualitative trends that become quite clear upon inspection of the data.

The positive secondary ion polarity depth profile of the control sample, indicated by the solid lines of Figure 2A, reveals that there is a relatively thick surface layer of sirolimus. The depth profile acquisition was carried out to a total depth of approximately 2.8 μm from the surface of the coating. At approximately 0.65 μm below the surface the relative quantities of sirolimus and PLGA invert. The sodium signal peaks just below the surface and then reaches a nominally fixed concentration in the bulk of the coating. We make the assumption that this relative concentration of sodium ($\sim 2 \times 10^3$ counts/cycle), independent of the relative quantities of sirolimus and PLGA within a given slice of the film, is

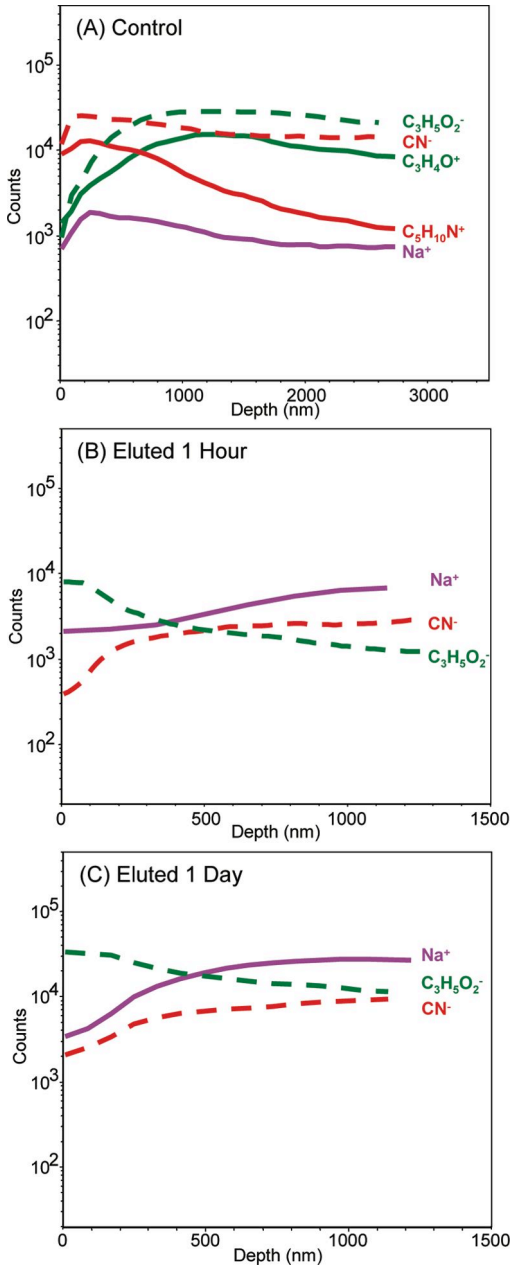

Figure 2. TOF-SIMS depth profiles showing signal intensity as a function of C_{60}^+-sputtered depth. Each sample was composed of 25% (w/w) sirolimus in PLGA. In each depth profile, the characteristic signals in the positive polarity are $C_5H_{10}N^+$ (sirolimus, solid red), $C_3H_4O^+$ (PLGA, solid green), and Na^+ (sodium, solid purple), and characteristic signals in the negative polarity are CN^- (sirolimus, dashed red) and $C_3H_5O_2^-$ (PLGA, dashed green). Note that only the negative polarity profiles, and the positive polarity profile of Na^+, are shown for the one-hour and one-day elution samples. (A) Control (time zero) sample depth profiles to total depths of approximately 2.8 and 2.6 μm in the positive and negative polarities, respectively. (B) One-hour elution sample depth profiles to total depths of approximately 1.1 and 1.3 μm in the positive and negative polarities, respectively. (C) One-day elution sample depth profiles to total depths of approximately 1.2 and 1.1 μm in the positive and negative polarities, respectively.

representative of the sodium concentration throughout the coating. The negative secondary ion polarity depth profile of the control sample, indicated by the dashed lines of Figure 2A, also reveals the presence of a relatively thick surface layer of sirolimus. This depth profile was carried out to a total depth of approximately 2.6 μm from the surface. Again, at approximately 0.6 μm below the surface the relative quantities of sirolimus and PLGA invert.

At each analytical cycle of the depth profile the lateral distribution of each chemical constituent is imaged, and these 2D images-at-depth may be extracted from the data file at any specified depth interval. In Figure 3 a series of five equidistant images from the depth profiles of the elution coating, in each secondary ion polarity, are displayed. Each image frame is a false color overlay of the sirolimus signal in red and the PLGA signal in green, and the intensity scale of each image is adjusted independently for best contrast. Chemical images of $C_5H_{10}N^+$ and $C_3H_4O^+$ represent the distribution of sirolimus and PLGA, respectively, in the positive secondary ion polarity, whereas chemical images of CN^- and $C_3H_5O_2^-$ represent the distribution of sirolimus and PLGA, respectively, in the negative secondary ion polarity. At the outset, one notices that the coatings are quite heterogeneous. In other words, the morphology of the elution coating varies substantially from one position to the next. Nevertheless, as deduced from the depth profile data, both sets of images reveal a surface that is composed largely of drug-rich areas. Sodium (not shown) is rather uniformly dispersed in the surface region of the sample; there is no localization of sodium to any discernible feature.

The images-at-depth in Figure 3 also reveal that the lateral distribution of sirolimus and PLGA, as well as the fractional composition of each component, changes as a function of depth from the surface of the coating. These image sets also highlight the morphological variation that is present within different portions of the coating. In the positive polarity (Figure 3A–E), a fissure, which is composed primarily of PLGA, extends into the bulk of the coating. Below the surface, interwoven fissure-like features are exposed and are observed to extend over approximately half of the image area. In the negative polarity (Figure 3F–K), a more phase-segregated structure of the sirolimus and the PLGA components is observed. Below the drug-rich surface layer, the domains of drug become smaller, whereas the domains of excipient become larger. At a depth of 2.6 μm, the excipient domains cover >80% of the image area. We also note, though it is not obvious from the 2D images because of the intensity scaling, that areas consisting primarily of PLGA contain a considerable quantity of sirolimus, whereas areas consisting primarily of sirolimus contain very little PLGA.

A set of 3D images of the control sample, constructed from the 2D images at each cycle of the negative polarity depth profile, are rendered in Figure 4. The corresponding 2D images-at-depth were displayed, in part, in Figure 3F–K. The 3D images are isosurface overlays of the CN^- (sirolimus, red) and $C_3H_5O_2^-$ (PLGA, green) signals. Isosurface modeling is a valuable method of 3D chemical imaging because multiple components may be imaged together, and the opacity of each layer may be reduced to view the interior of the image volume. Before generation of each isosurface, an intensity threshold is selected by the user. This allows, for instance, the exclusion of low-intensity pixels so that the salient features of the chemical distributions may be easily identified. The 3D images confirm

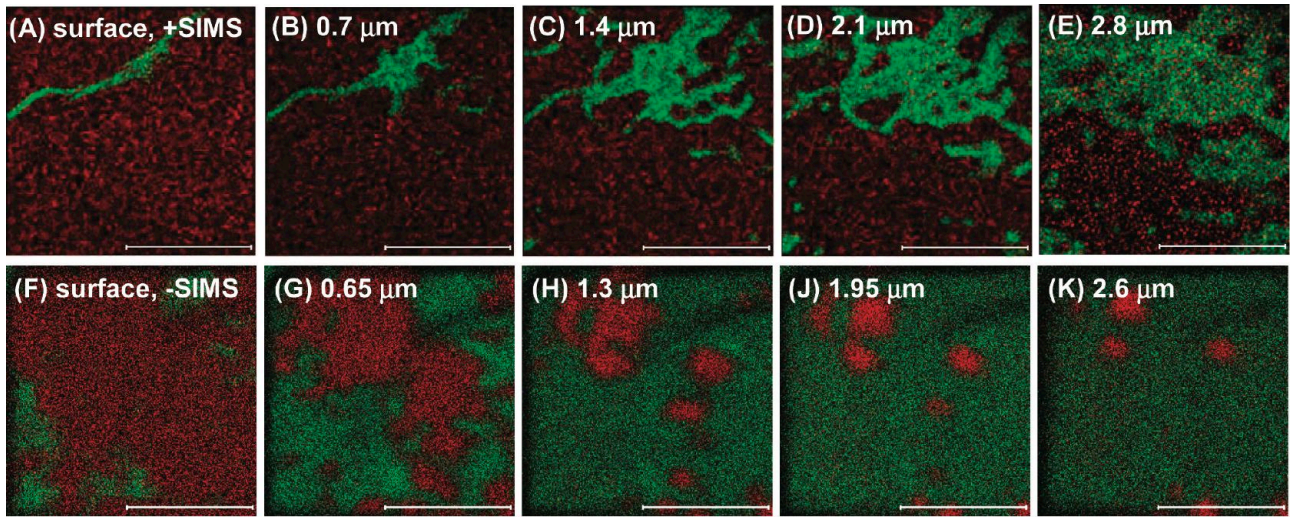

Figure 3. TOF-SIMS 2D images-at-depth extracted at equidistant intervals from the depth profile data shown in Figure 2A. The field of view of each image is 200 μm $\times$ 200 μm. The approximate distance from the surface is indicated on the respective images. (A−E) Positive polarity overlay images of $C_5H_{10}N^+$ (sirolimus, red) and $C_3H_4O^+$ (PLGA, green). (F−K) Negative polarity overlay images of CN^- (sirolimus, red) and $C_3H_5O_2^-$ (PLGA, green).

certain deductions regarding the structure of the elution coating which were initially based on the depth profiles and the 2D images-at-depth. The most obvious are a drug-rich surface layer and a more phase-segregated distribution of drug below the surface. One should be aware that the porous appearance of the sirolimus surface layer, viewed in Figure 4A, is a consequence of the threshold setting that was chosen to amplify the subsurface domain structure. Nevertheless, the 3D images allow one to elucidate the nuances of the unexpectedly complex subsurface chemical distribution. For instance, in Figure 4B, which is rotated to reveal two sides of the image volume, it is clear that the subsurface structure is not a simple phase segregation of drug and excipient. Rather, the subsurface drug distribution includes drug-rich channels that extend from the surface layer into the bulk of the elution coating. In Figure 4C, the 3D image volume, viewed from the side, is displayed with the opacity of the PLGA isosurface having been reduced. This view clearly reveals both the sirolimus-rich surface layer and the channels extending into the excipient. In this rendering, two additional features of the chemical distribution are illuminated; these features include a region below the surface that is somewhat depleted of sirolimus which is followed by a more particulate dispersion of the drug in the polymer matrix. These observations are confirmed by XPS analysis which is discussed below. But we may also produce region-of-interest (ROI) depth profiles from the TOF-SIMS raw data file to distinguish the concentration gradients of both sirolimus and PLGA at different points of the 3D image volume.

Region-of-interest depth profiles were generated from two different areas of the control sample in the negative secondary ion polarity, and the results of these ROI depth profiles are furnished in Figure 5. Each ROI is approximately 70 μm square. The first ROI, indicated on the inset of Figure 5A, was acquired from an area of the sample having a drug-rich surface and a high density of drug-enriched subsurface channels. The resulting depth profiles of CN^- (sirolimus, red) and $C_3H_5O_2^-$ (PLGA, green) do not indicate a depletion layer but an increase in the concentration of PLGA as the subsurface channels of sirolimus taper and extinguish as a function of depth (refer to Figure 4C, right side). The second ROI, identified on the inset of Figure 5B, was acquired from an area of the sample having a drug-rich surface and only a couple short drug-enriched subsurface channels. The resulting depth profiles of CN^- (sirolimus, red) and $C_3H_5O_2^-$ (PLGA, green) reveal a subsurface layer with a reduced concentration of sirolimus and a corresponding increase in the concentration of PLGA. Beyond the drug depletion layer, the quantity of sirolimus again increases which corresponds to the particulate dispersion observed in the 3D image volume (refer to Figure 4C, left side).

Confocal Raman microscopy was performed on a control sample (25 wt % sirolimus in PLGA), and the resulting images, showing a vertical cross section of 60 μm $\times$ 5 μm perpendicular to the surface, are given in Figure 6. The images of parts A and B of Figure 6 show the signals of sirolimus and PLGA, respectively, on a thermal scale. A false color overlay is given in Figure 6C which shows the sirolimus (red) and PLGA (green) signals of the elution coating. The Raman images show interesting chemical morphology which correlates well with the morphology seen in the TOF-SIMS images, though one should bear in mind that the Raman cross section is 65 μm wide, whereas the TOF-SIMS images are 200 μm wide. Upon examination of the outer surface, ignoring the slight thickness variations, the Raman images show the surface to have large areas rich in sirolimus and smaller areas rich in PLGA exhibiting the two-phase structure observed in the TOF-SIMS images. About 0.6 μm into the coating, the TOF-SIMS depth profiles indicate that, averaged over the image area, the overall composition of the coating switches from richer in sirolimus to richer in PLGA. On a comparable scale, the Raman images show a transition from a drug-enriched surface to regions enriched in the polymer. Also, there appear to be discontinuities, or fissures, in a couple areas of the sirolimus-rich surface which

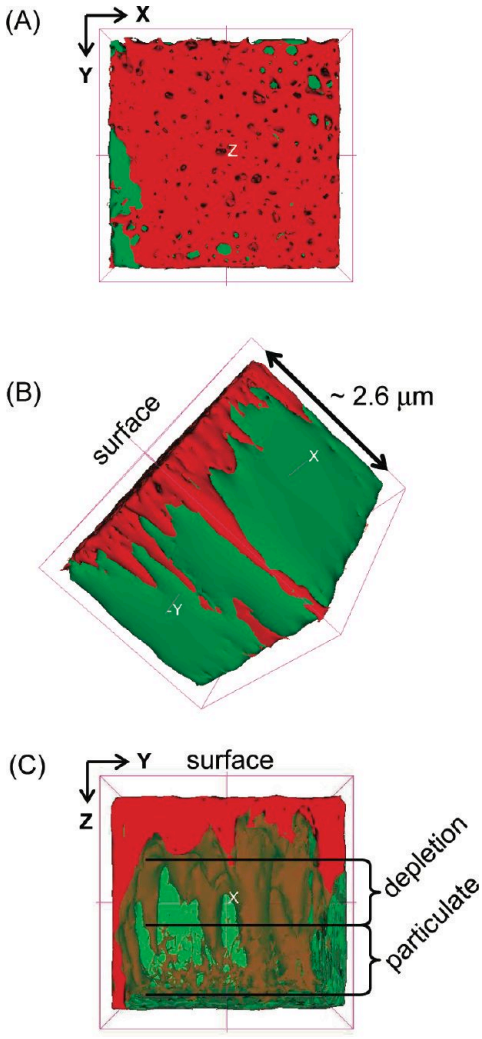

Figure 4. TOF-SIMS 3D images of the control sample acquired in the negative polarity. The field of view is 200 μm × 200 μm, and the approximate depth of the image volume is 2.6 μm. (A) Isosurface overlay of CN^- (sirolimus, red) and $C_3H_5O_2^-$ (PLGA, green) showing the surface view. (B) Isosurface overlay of CN^- (sirolimus, red) and $C_3H_5O_2^-$ (PLGA, green) showing a side view between the $+X$ and $-Y$ axes. (C) Isosurface overlay of CN^- (sirolimus, red) and $C_3H_5O_2^-$ (PLGA, green) showing a view along the $+X$ axis. The opacity of PLGA has been reduced to 0.5 so that the interior of the image volume may be observed.

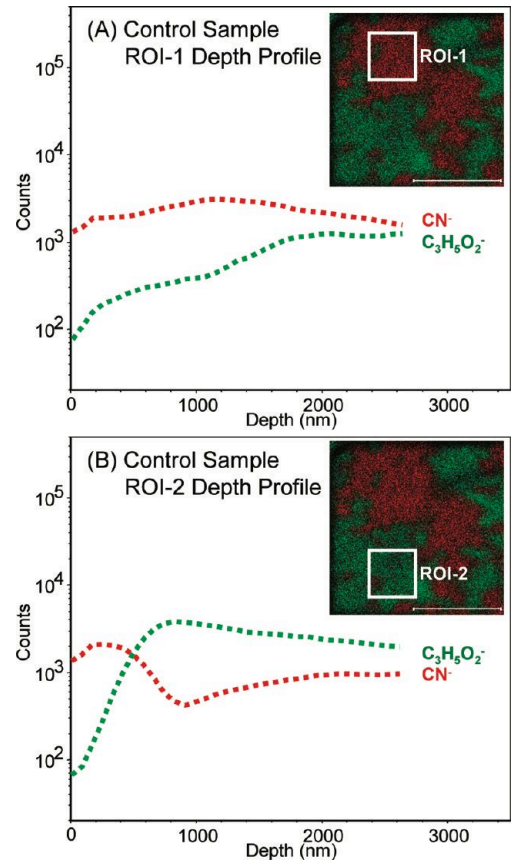

Figure 5. TOF-SIMS region-of-interest (ROI) depth profiles, extracted from two different areas within the 200 μm × 200 μm negative polarity depth profile of the control sample, showing signal intensity as a function of C_{60}^+-sputtered depth. For each 70 μm × 70 μm ROI indicated on the respective inset, the depth profiles of CN^- (sirolimus, red) and $C_3H_5O_2^-$ (PLGA, green) are given. (A) ROI-1 was acquired from an area of the sample having a drug-rich surface and a high density of drug-enriched subsurface channels. (B) ROI-2 was acquired from an area of the sample having a drug-rich surface and insignificant drug-enriched subsurface channels.

may be similar to those observed by TOF-SIMS (Figure 3A–E). Below the drug-rich surface, the Raman images show domains of drug enrichment dispersed in a polymer-enriched continuum as was observed by TOF-SIMS (Figure 3F–3K). Upon further examination of the Raman images, small channels enriched in sirolimus appear to extend from the sirolimus-rich regions of the surface into the PLGA-rich regions below the surface. These channels of drug are near the resolution limit of the Raman method and appear smaller than some of the channels observed by TOF-SIMS (Figure 4). Although the coating appears to exhibit region-to-region differences in the dimensions of the chemical morphologies, the confocal Raman microscopy and TOF-SIMS images exhibit qualitatively similar features on a comparable size and depth scale.

A depth profile of a control sample (50 wt % sirolimus in PLGA) was obtained by means of XPS in conjunction with C_{60}^+ ion beam sputtering. The depth profile data are provided in Figure 7. In addition to the difference in sirolimus concentration, the film examined by XPS was spin-cast from solution onto the metal coupon rather than spray-coated. The XPS profile data, which are the result of a single analysis, bear meaningful insight to the present study. The depth distribution of sirolimus is uniquely identified by the profile of nitrogen (red) because there is no nitrogen in the molecular structure of PLGA. The depth distribution of PLGA is indicated by the profile of oxygen (green), though not uniquely, because there is a higher fraction of oxygen in the molecular structure of PLGA than that of sirolimus. The depth profile of carbon seems to emulate the distribution of the drug, or nitrogen, near the surface because of the relatively high abundance of drug toward the surface. However, beyond the surface region the depth profile of carbon seems more representative of the 50:50 (w/w) composition of the drug and excipient. The presence of an adventitious surface layer of silicone, and the C_{60}^+ sputter removal of this contaminant to expose the underlying elution coating, is established by the depth profile of silicon. It should be noted that the signal of sodium was below the detection limit of the survey scan and so was not monitored in the depth profile.

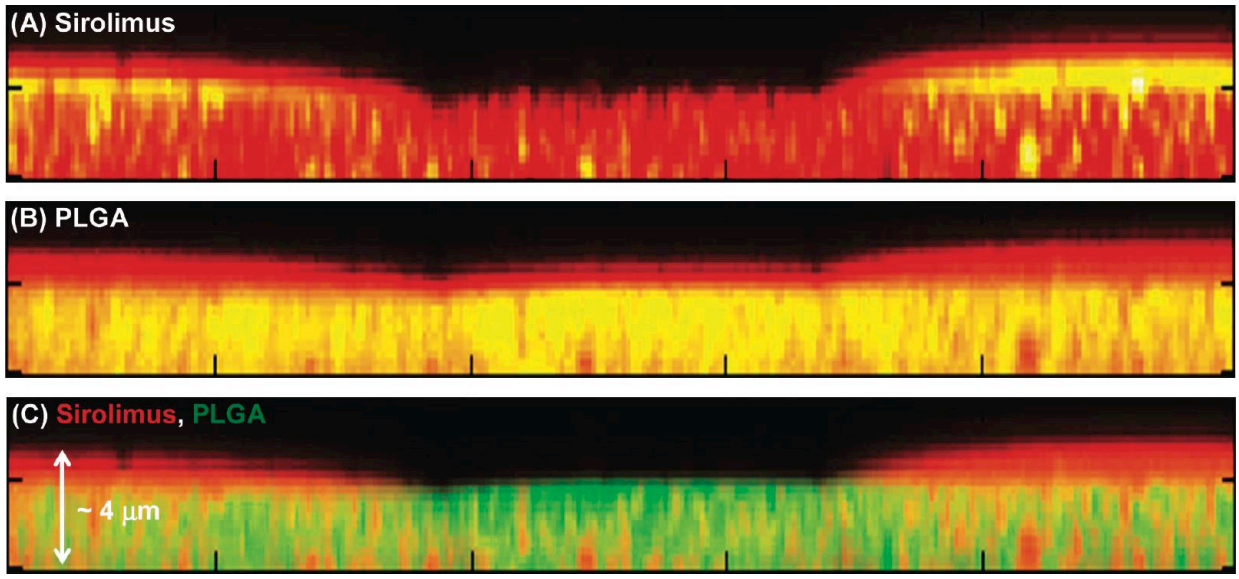

Figure 6. Confocal Raman microscopy images showing a cross-sectional reconstruction perpendicular to the surface of the spray-applied control (time zero) coating of 25% (w/w) sirolimus in PLGA; the total image area is 60 μm × 5 μm: (A) sirolimus image, thermal scale; (B) PLGA image, thermal scale; (C) overlay image of sirolimus (red) and PLGA (green).

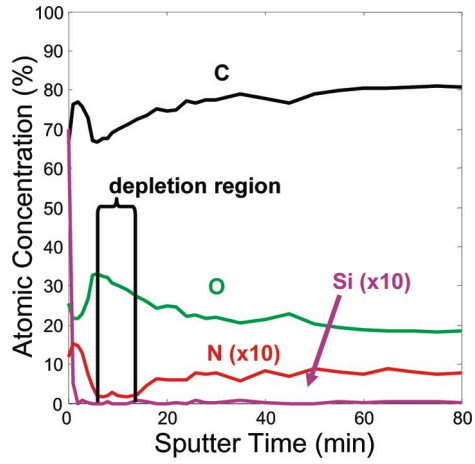

Figure 7. XPS depth profile of a spin-cast 50% (w/w) sirolimus in PLGA elution coating showing atomic concentrations of carbon (black), nitrogen (red), oxygen (green), and silicon (purple) as a function of C_{60}^+ sputter time. The total sputtered depth is approximately 0.8 μm.

The XPS depth profile data (Figure 7), specifically of nitrogen and of oxygen, reveal a surface that is composed predominantly of sirolimus followed by a region that is depleted of the drug. Beyond the drug-depleted region, a relatively uniform distribution of drug and excipient is observed. The observation of a subsurface region that is depleted of sirolimus was a striking characteristic of the 3D TOF-SIMS images that is confirmed by both XPS depth profiling and TOF-SIMS ROI depth profiling. The difference between the results of XPS and TOF-SIMS concerning the depletion region is the depth at which the depletion occurs. The TOF-SIMS ROI depth profile indicates a depletion zone at a depth of ~0.6 μm, whereas the XPS depth profile indicates a depletion zone at a depth of ~0.1 μm. We presume that this difference is related to the heterogeneity, or morphological variation, within each sample. It is interesting to note that the thickness of the drug-enriched surface layer and the depth of the depletion region does not seem to correspond with the weight fraction of sirolimus in the samples used for TOF-SIMS and XPS analysis, i.e., 25% and 50%, respectively. However, the application method of the drug/excipient films may be the primary factor in the observed depth of the drug depletion region as well as the thickness of the drug-enriched surface layer.

TOF-SIMS depth profiles of the one-hour elution sample, given in Figure 2B, were carried out in the positive and the negative secondary ion polarities to total depths of 1.1 and 1.3 μm from the surface, respectively. For ease of comparison and discussion, only the CN^-, $C_3H_5O_2^-$, and Na^+ profiles are presented. The profiles of CN^- (sirolimus, red) and $C_3H_5O_2^-$ (PLGA, green) indicate that there is much less sirolimus at the surface and that there is a rather uniform distribution of drug and excipient at depths of >0.5 μm from the surface. The Na^+ (purple) profile indicates that, in comparison to the control sample, there is more sodium in the surface region and, on average, there is an order of magnitude more sodium in the bulk of the film. This observation makes sense in light of the fact that the elution medium contains sodium; as sirolimus is eluted from the coating, sodium remains.

The corresponding 3D TOF-SIMS images of the one-hour elution sample, showing the isosurfaces of $C_5H_{10}N^+$ (sirolimus, red), $C_3H_4O^+$ (PLGA, green), and Na^+ (purple), are rendered in Figure 8. Note that we switch here to using positive polarity secondary ions specifically to reveal the 3D localization of sodium. Due to the inherent heterogeneity of the sample, imaging the 3D localization of sodium may only be accomplished with respect to the signals of sirolimus and PLGA in the same secondary ion polarity. From the isosurface overlays in Figure 8, parts A and B, it can be seen that the remaining surface layer of sirolimus is quite thin and porous, and beyond the surface the remaining drug is more evenly dispersed through the excipient than was observed in the images of the control sample. Moreover, there is no evidence of a subsurface layer depleted of sirolimus in the one-hour elution sample. These observations are consistent with

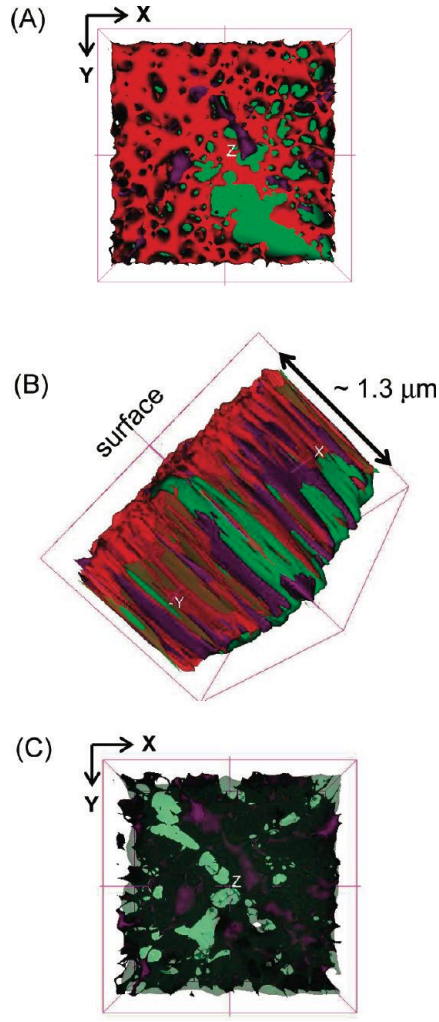

Figure 8. TOF-SIMS 3D images of the one-hour elution sample acquired in the positive polarity. The field of view is 200 μm $\times$ 200 μm, and the approximate depth of the image volume is 1.3 μm. (A) Isosurface overlay of $C_5H_{10}N^+$ (sirolimus, red), $C_3H_4O^+$ (PLGA, green), and Na^+ (purple) showing the surface view. (B) Isosurface overlay of $C_5H_{10}N^+$ (sirolimus, red), $C_3H_4O^+$ (PLGA, green), and Na^+ (purple) showing a side view between the $+X$ and $-Y$ axes. (C) Isosurface overlay of $C_3H_4O^+$ (PLGA, green) and Na^+ (purple) showing the surface view. The opacity of PLGA has been reduced to 0.5 so that the interior of the image volume may be observed.

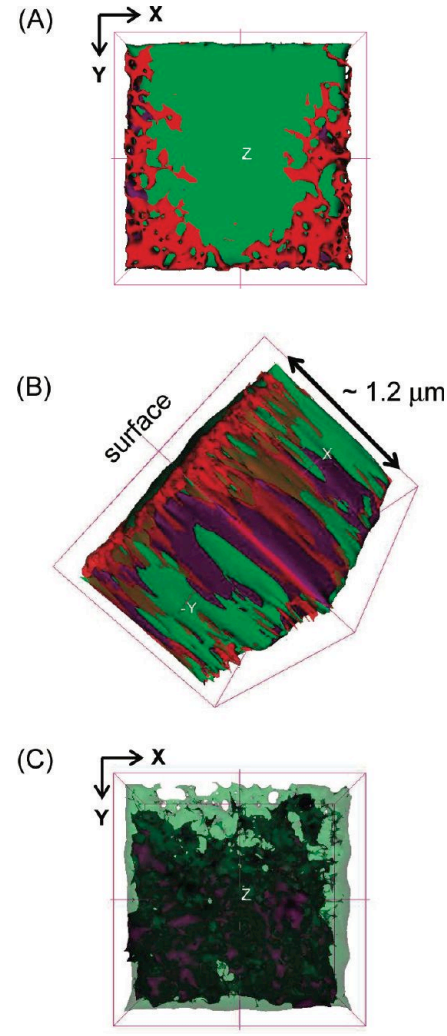

Figure 9. TOF-SIMS 3D images of the one-day elution sample acquired in the positive polarity. The field of view is 200 μm $\times$ 200 μm, and the approximate depth of the image volume is 1.2 μm. (A) Isosurface overlay of $C_5H_{10}N^+$ (sirolimus, red), $C_3H_4O^+$ (PLGA, green), and Na^+ (purple) showing the surface view. (B) Isosurface overlay of $C_5H_{10}N^+$ (sirolimus, red), $C_3H_4O^+$ (PLGA, green), and Na^+ (purple) showing a side view between the $+X$ and $-Y$ axes. (C) Isosurface overlay of $C_3H_4O^+$ (PLGA, green) and Na^+ (purple) showing the surface view. The opacity of PLGA has been reduced to 0.5 so that the interior of the image volume may be observed.

contraction of the coating following elution as noted by Belu et al.[2] Some deposits of sodium are observed at the surface which seem highly correlated to areas of sirolimus remaining at the surface. In Figure 8C, the isosurface of sirolimus was excluded and the opacity of the PLGA isosurface was reduced so that the interior distribution of sodium is easily examined. What is striking is that a significant portion of the sodium distribution appears in columnar formations below the surface with little appearing at the surface. We speculate that these columnar aggregates of sodium occur in subsurface channels that were previously occupied by sirolimus. Regarding the relatively low concentration of sodium at the surface, we suppose that sodium remains solvated when the sample is extracted from the elution medium. The subsurface sodium is trapped by contraction of the coating.

The depth profiles of the one-day elution sample, shown in Figure 2C, were carried out in the positive and the negative secondary ion polarities to total depths of 1.2 and 1.1 μm from the surface, respectively. Again, only the CN^-, $C_3H_5O_2^-$, and Na^+ profiles are presented. The profiles of CN^- (sirolimus, red) and $C_3H_5O_2^-$ (PLGA, green) indicate much less sirolimus at the surface and in the bulk compared to the one-hour elution sample. The Na^+ (purple) profile reveals even higher concentrations of sodium in the near-surface and bulk regions of the film ostensibly as a result of the longer elution time. The corresponding 3D images of the one-day elution sample are given in Figure 9. From the isosurface overlays of $C_5H_{10}N^+$ (sirolimus, red), $C_3H_4O^+$ (PLGA, green), and Na^+ (purple) it can be seen that little remains of the drug-rich surface layer. What sirolimus remains beyond the surface appears in the coating as a dispersion with some particulate domains. At the surface, again, deposits of sodium appear correlated with areas of remaining sirolimus. In Figure 9C the isosurface of sirolimus has been excluded and the opacity of the PLGA isosurface has

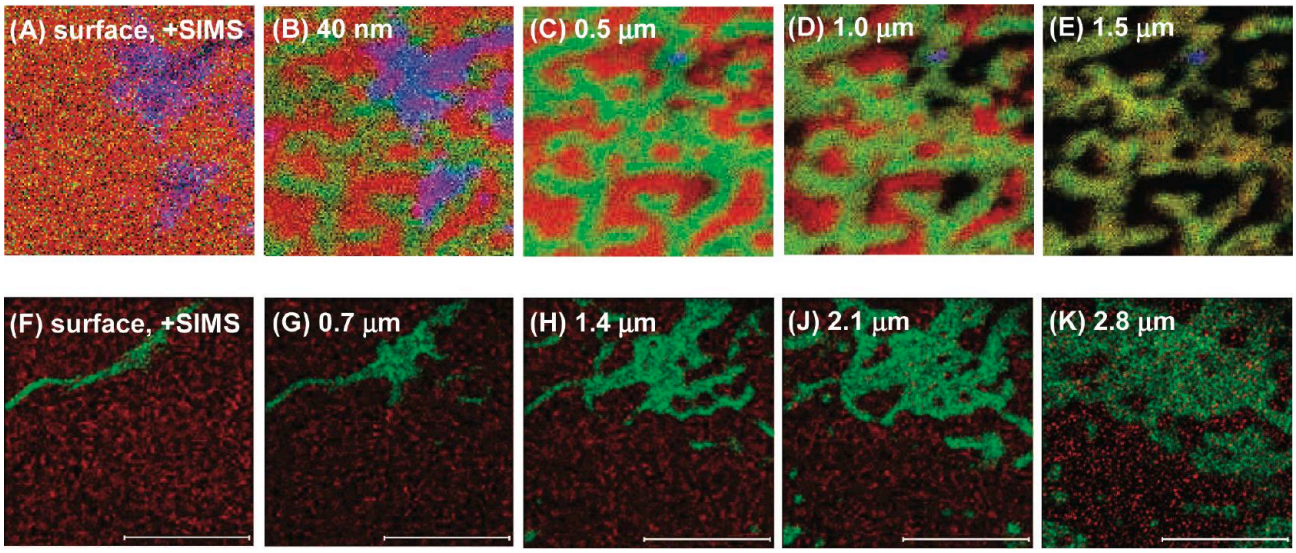

Figure 10. TOF-SIMS 2D images-at-depth extracted from depth profile data that was acquired using different dc sputter ion sources. The field of view of each image is 200 μm $\times$ 200 μm. The approximate distance from the surface is indicated on the respective images. (A−E) Positive polarity overlay images of $C_5H_{10}N^+$ (sirolimus, red), $C_3H_4O^+$ (PLGA, green), and K^+ (potassium, purple). Images were acquired with 5 kV SF_5^+ sputtering while the sample was held at −100 °C. (F−K) Positive polarity overlay images of $C_5H_{10}N^+$ (sirolimus, red) and $C_3H_4O^+$ (PLGA, green). Images were acquired with 20 kV C_{60}^+ sputtering and the sample at room temperature.

been reduced so that the bulk distribution of sodium may be elucidated. In this specimen there are no columnar-type deposits of sodium observed but, rather, a more random distribution over a larger portion of the image volume. Again, this behavior may be explained by, and is not inconsistent with, contraction of the coating during elution as noted previously.

To summarize the data from the control (time zero) sample, the one-hour, and the one-day elution samples, presented in Figures 2−9, we observe that the as-deposited surface of the control sample is composed of large areas that are enriched in the drug. The surface morphology is quite variable with some areas that are relatively homogeneous and other areas that contain features which appear as fissures. Moreover, in areas of the surface that appear to have a uniform layer of the drug, i.e., no features such as fissures, the thickness of the drug-enriched layer is observed to be variable. Below certain areas of the sirolimus-enriched surface there is a region that is somewhat depleted of the drug. Beneath other areas of the drug-enriched surface, there are drug-enriched channels that penetrate through the depletion region into the bulk. It is unclear whether or not the depth of the depletion region, or the relative concentration of drug in the depletion region, bears any dependence on the thickness of the drug-enriched surface layer because we have not performed a controlled study of this trend; however, the application method (i.e., spray-coated or spin-cast) does seem to have a significant impact on the early elution rate of the drug. Beyond the drug-depleted region the distribution of the drug in the excipient varies. The bulk distribution of the drug is observed as phase-segregated domains, or grains, of drug as well as areas of relatively uniform dispersion. In general, it seems that regions of PLGA are saturated with sirolimus, whereas regions consisting primarily of sirolimus contain very little PLGA. With the onset of elution, drug elutes on a short time scale from the surface and from within the drug-enriched subsurface channels. This mechanism is evidenced by alkali ions that remain in the channels following elution, though there is little evidence of sodium at the surface following elution. We hypothesize that there is little sodium at the surface because it remains in solution when the sample is extracted from the elution medium, and the subsurface deposits of sodium arise because the coating contracts during the elution process. Elution of the drug from phase-segregated and dispersed phases occurs on a longer time scale.

There are intrinsic characteristics associated with an energetic C_{60}^+ molecular ion beam that are unique among the sputter ion beams available to achieve depth profiling of an organic matrix. These unique qualities have facilitated the 3D imaging by TOF-SIMS that was discussed above. The salient characteristics of C_{60}^+ ion sputtering are described by the sputtered volume, the range (i.e., penetration depth), and the relative inertness of incident C_{60}^+ ions toward the sputtered organic matrix. The combined attributes of a large sputtered volume and a small penetration depth result in very little residual chemical damage imparted to the sample matrix.[9−13] Though some chemical damage remains in the sample matrix it is removed by subsequent C_{60}^+ ion impact events. Thus, steady-state molecular depth profiling is achieved because residual chemical damage comprises only a small portion of the subsequently sampled chemistry. This phenomenon is highlighted with data collected in the present study from a set of control samples using different sputter ion beams.

Two sets of 2D images-at-depth, extracted from depth profile data collected in the positive secondary ion polarity, are rendered in Figure 10. Each image frame is a false color overlay exposing the lateral distributions of sirolimus ($C_5H_{10}N^+$, red) and PLGA ($C_3H_4O^+$, green). The top row of images also show the distribution of potassium (K^+, blue), an element that was not present in significant quantities on the area of the sample shown in the bottom row of images. The images of Figure

(13) Delcorte, A.; Garrison, B. J. *Nucl. Instrum. Methods Phys. Res., Sect. B* **2007**, *225*, 223–228.

10A−E were collected using an SF_5^+ ion beam for dc sputtering during the depth profile acquisition as described in the Experimental Section. Additionally, the sample temperature was nominally maintained at −100 °C during the depth profile analysis to minimize the sputter ion-induced artifacts and to achieve nominal uniformity in the sputter rate. The images of Figure 10F−K were collected using a C_{60}^+ ion beam for dc sputtering during the depth profile acquisition as described in the Experimental Section, and the sample temperature was nominally held at room temperature for the duration of the analysis. These data provide an ideal means for differentiating the capabilities of different polyatomic sputter ion sources in a practical analytical application. The expediency of this comparison arises not only because the samples were produced in the same manner but also because the areas of each sample that were imaged have a very similar morphology.

Each area of the analyzed samples begins with a surface that is enriched in sirolimus. Beyond the surface, interwoven fissure-like features are exposed which evolve to extend over approximately half of the imaged area. What is noteworthy is that, in the case of C_{60}^+ ion sputtering (Figure 10F−K), the characteristic signals of both the drug and the excipient remain through the entire profile depth of 2.8 μm. However, in the case of SF_5^+ ion sputtering (Figure 10A−E), the characteristic signal of sirolimus degrades. The degradation of the sirolimus signal is recognizable at a depth of ~0.5 μm, and at a depth of 1.5 μm the characteristic signal of sirolimus is observed only in the PLGA-rich regions of the matrix. The proclivity of sirolimus toward ion beam-induced damage has been recognized previously.[7] In the present case, we have demonstrated a minimum 6-fold increase in the information depth with the use of a C_{60}^+ sputter ion beam. Additionally, we have confirmed by practical analytical application that differences in the physics of sputtering between monatomic and polyatomic ion beams (e.g., Ar^+, O_2^+, Cs^+, and SF_5^+) and a molecular ion beam (e.g., C_{60}^+) are important; namely, a condition of steady-state organic depth profiling requires that the sputtered volume is greater than the penetration depth.[9−14] This condition is met in the current study by sputtering with a C_{60}^+ ion beam.

CONCLUSIONS

We have reported the first full 3D visualization of the chemical constituents in a pharmaceutical bearing coronary stent coating as a function of elution time. The 3D chemical imaging was accomplished by TOF-SIMS imaging in conjunction with a C_{60}^+ ion beam for sputter depth profiling. The TOF-SIMS technique bridges an analytical imaging gap by combining high lateral resolution with molecular specificity. However, XPS depth profiling and confocal Raman microscopy were also applied in this study for bulk compositional analysis of the pristine coronary stent coating. The complementary nature of the XPS and confocal Raman analyses confirmed certain features in the 3D TOF-SIMS images and substantiated the conclusions based on the 3D TOF-SIMS images.

In summary, the 25% (w/w) formulation of sirolimus in PLGA examined in this study is shown to have large areas of the surface as well as subsurface channels that are composed primarily of the drug, followed by a drug-depleted region and, finally, a relatively homogeneous dispersion of the drug in the polymer matrix. Below the surface, areas composed primarily of PLGA have a considerable quantity of sirolimus but areas composed primarily of sirolimus contain very little PLGA. Elution is shown to occur from the drug-enriched surface region on a relatively short time scale and more gradually from subsurface regions of homogeneous drug dispersion. We surmise that the application method of the drug/excipient formulation, e.g., spray-applied or spin-cast, has a profound effect on the early elution rate of drug from the coating. Finally, during the initial stages of elution, the drug is also evolved from the subsurface channels that are enriched in the pharmaceutical. This observation is inferred by the alkali species (e.g., Na^+) that remain in these channels following the first hour of elution.

We have also assessed the efficiencies of a C_{60}^+ molecular ion beam together with a SF_5^+ polyatomic ion beam for TOF-SIMS 3D imaging. This assessment was conducted in a rather qualitative manner since the analyses were performed on different instruments; however, the results are in accordance with more controlled studies reported in the literature. The C_{60}^+ molecular ion beam is demonstrated to be a superior sputter source for 3D TOF-SIMS imaging applications because it combines a large sputtered volume and a small penetration depth that results in very little residual chemical damage imparted to the sample matrix. This residual chemical damage is removed, and undamaged material is sampled, by subsequent C_{60}^+ ion impact events resulting in a steady-state molecular depth profile. In other words, C_{60}^+ ion beam-induced damage to the matrix is greatly reduced compared to that produced by the SF_5^+ ion beam. Therefore, C_{60}^+-based 3D image acquisitions continued well beyond the depth at which the characteristic sirolimus signal diminished in the SF_5^+-based acquisitions. A further consequence of this difference is that C_{60}^+-based 3D image acquisitions were able to be performed with the sample at room temperature, whereas the corresponding SF_5^+-based acquisitions required the sample to be maintained at −100 °C. It is hypothesized that the reduced temperature moderates the potential of SF_5^+ ion beam-induced radicals in the sample matrix to produce further damage.

ACKNOWLEDGMENT

We thank Phillip McDonald and Chris Hobot, both of Medtronic, for their work in preparing the samples and performing the elution study. Certain commercial equipment, instruments, or materials are identified in this article to specify adequately the experimental procedure. Such identification does not imply recommendation or endorsement by the National Institute of Standards and Technology, nor does it imply that the materials or equipment identified are necessarily the best available for the purpose.

SUPPORTING INFORMATION AVAILABLE

Additional information as noted in text. This material is available free of charge via the Internet at http://pubs.acs.org.

Received for review July 16, 2009. Accepted October 25, 2009.

AC901587K

(14) Kollmer, F. *Appl. Surf. Sci.* **2004**, *231−232*, 153–158.